Modeling of Hydraulic Fracturing in a Poroelastic Cohesive Formation

E. Sarris, Ph.D.[1]; and P. Papanastasiou[2]

Abstract: This paper investigates the main parameters that affect the propagation of a fluid driven-fracture in a poroelastic medium. The fracture results from the pumping of an incompressible Newtonian viscous fluid at the fracture inlet, and the flow in the fracture is modelled by the lubrication theory. Rock deformation is assumed as porous-elastic. Leak-off in the host rock is considered to account for the diffusion effects in the surrounding formation. The propagation criterion is of the cohesive type. Finite element analysis was performed to compute the fracturing pressure and fracture dimensions as a function of the time and length. It was found that higher pressures are needed to extend a fracture in a poroelastic medium than in an elastic medium, and the created profiles of poroelastic fracture are wider. It was found that grain compressibility plays a minor role and does not result any significant difference in the fluid pressures and fracture dimensions. Wider fracture profiles are obtained with higher injection rates. The fluid pressures and the fracture apertures are larger in the case of a high permeability formation. **DOI: 10.1061/(ASCE)GM.1943-5622.0000121.**

CE Database subject headings: Hydraulics; Cracking; Finite element method; Poroelasticity.

Author keywords: Hydraulic fracturing; Poroelastic formation; Net-pressure; Cohesive zone; Coupled problems; Finite elements.

Introduction

Hydraulic fracturing (HF) can be grossly defined as the process in which a fracture initiates and propagates with the application of hydraulic loading (pressure) induced on the fracture walls by a viscous fluid. The purpose is to enhance recovery of the hydrocarbons through a highly conductive channel that is created. A good example is the recent production of hydrocarbons from unconventional resources such as low permeability shales, which is made possible through the HF technique. The engineers have tamed the capabilities of the HF and applied it also to other engineering disciplines. In mining engineering, HF is used for the preconditioning of ore rock masses in mining operations to promote caving (Jeffrey et al. 2001). In environmental engineering, HF may be used for the formation of barriers to stop contaminant transport in environmental projects (Murdoch and Slack 2002). Another application is the reinjection of drilling cuttings and more recently the CO_2 sequestration (Logan et al. 2000). In geothermal reservoirs, the technique is used for heat production (Legarth et al. 2005). In geotechnical engineering, HF is used to compensate grouting to offset the effects of subsidence beneath buildings.

The mathematical description of the hydraulic fracturing technique is the problem of the fluid driven fracture. This problem is widely used in the petroleum industry to develop and calibrate numerical simulators that accurately predict the needed pressures and the dimensions of the created fracture. Over the years, this problem has attracted numerous research contributions that have been oriented toward the understanding of the mathematical physics of the fluid-driven problem by using rigorous and complex analysis (Desroches et al. 1994; Carbonell et al. 1999; Garagash and Detournay 2000; Savitski and Detournay 2002; Detournay 2004; Zhang et al. 2005; Lecampion and Detournay 2007; Adachi and Detournay 2008).

In field operations, attention is focused on the prediction of the wellbore pressure, which is normally measured during the treatment and is usually the only parameter available to evaluate the operation. Classical hydraulic fracturing simulators often underestimate the measured downhole pressures. Research works involving surveying on net-pressures (difference between fracturing fluid pressure and the far-field confining stress) indicated that the net-pressures encountered in the field are on average 50–70% more than the predicted ones. These observations have triggered a series of dedicated studies that looked into the importance of the rock plastic deformation in hydraulic fracturing (Papanastasiou and Thiercelin 1993; Papanastasiou 1997; Germanovich et al. 1998; Papanastasiou 1999a; Van Dam et al. 2002). All these studies had ignored the pressure diffusion and porous behavior of the rock deformation.

In this research work, the influence of some main parameters are investigated that affect the propagation of a fluid-driven fracture in a poroelastic medium. These parameters include the injection rate, the formation permeability, and the formation compressibility. The main objective is to explain, at least partially, the unexpected high fluid pressures observed in hydraulic fracturing field operations. This paper is organized in two parts as follows: In the first part, the involved physical processes are described: the fluid-flow, the rock deformation, and fracture propagation, and the numerical implementation. In the second part, the obtained computational results are presented and critically evaluated.

Methodology

The physical process of the fluid driven fracture involves the pumping of a viscous fluid that pressurizes the fracture surfaces which

[1]Dept. of Civil and Environmental Engineering, Univ. of Cyprus, P.O. Box 20537, 1678 Nicosia, Cyprus. E-mail: esarris@ucy.ac.cy

[2]Professor, Dept. of Civil and Environmental Engineering, Univ. of Cyprus, P.O. Box 20537, 1678 Nicosia, Cyprus (corresponding author). E-mail: panospap@ucy.ac.cy

Note. This manuscript was submitted on September 14, 2010; approved on February 9, 2011; published online on February 11, 2011. Discussion period open until September 1, 2012; separate discussions must be submitted for individual papers. This paper is part of the ***International Journal of Geomechanics***, Vol. 12, No. 2, April 1, 2012. ©ASCE, ISSN 1532-3641/2012/2-160–167/$25.00.

Int. J. Geomech., 2012, 12(2): 160-167

deform. Increasing the pressurization, critical stress conditions will be reached ahead of the tip splitting the rock and driving hydraulically the fracture. This process reveals that there is a strong coupling between the moving fluid, rock deformation and fracture propagation. Depending on the formation properties, in situ stresses and pumping parameters, the fracture may propagate for a few hundred meters. In this study the fracture will propagate few meters which will be enough to extrapolate and reach correct conclusions for short and long-fractures. The propagation of a short fracture can be used to interpret the results of the minifrac which is a calibration test that is carried out first in situ for determining parameters such as the formation permeability and the minimum geostatic stress that are further used for calibrating and modeling the main hydraulic fracture.

The simulation of the HF process is not a trivial task because it involves the coupling of at least four physical mechanisms: (1) the fluid-flow within the fracture, (2) the deformation of the surrounding medium induced by the fluid pressure on the fracture surfaces, (3) the leak-off of the fracturing fluid in the permeable medium, and (4) the fracture propagation.

Now, the fully coupled numerical model for a fluid driven fracture in a porous rock is described. The models were developed for plain strain geometry taking into consideration the symmetry conditions. Polar symmetry could be used only if the in situ horizontal stresses were equal and the vertical in situ stress was the minimum stress. These conditions, which are limited to shallow depths, would create a penny shape horizontal fracture perpendicular to the wellbore axis. The plain strain geometry is the most appropriate for modeling short fractures with fracture heights relatively large compared to the fracture length. Furthermore, this geometry is also appropriate for examining tip effects because the deformation near the tip of any arbitrary fracture shape is approximately planar. The fracture propagates perpendicular to the minimum in situ stress and remains planar. This predefined path for the propagation is also convenient for using the cohesive zone numerical approach.

Fluid-Flow

The fluids that are used in hydraulic fracturing are normally power-law with shear-thinning behavior, which means that the viscosity decreases with increasing shear strain rate. To avoid this complex fluid behavior, a simple appropriate model for fluid-flow in a fracture is embodied in the lubrication theory. It assumes laminar flow (uniformly viscous Newtonian), the fluid is incompressible and it accounts for the time-dependent rate of crack opening. The continuity equation, which imposes the conservation of mass in one dimensional flow, is as follows:

$$\frac{dq}{dx} - \frac{dw}{dt} + q_l = 0 \tag{1}$$

where, q = local flow rate along the fracture length x q_i = fluid loss in rock formation; and w = crack opening.

The second equation is derived from the conservation of linear momentum balance. For a fluid-flow between parallel plates the lubrication equation, which relates the pressure gradient to the fracture width for a Newtonian fluid of viscosity μ, yields to the following:

$$q = u.w = -\frac{w^3}{12\mu}\frac{dp}{dx} \tag{2}$$

where, p = fluid pressure; and u = average velocity of the fluid on a cross section in the fracture. Eq. (2) determines the pressure profile along the fracture from the local width and local flow rate. According to Eq. (2), the pressure gradient and hence the solution, is very sensitive to the fracture width variation. Therefore, the largest part of the pressure drop takes place within a small area near the tip where the width decreases significantly before it vanishes at the tip.

The fracturing fluid is assumed to be incompressible, and the flow boundary condition is imposed at the fracture mouth to meet the specific injection or flow rate (Neumann boundary condition). For the numerical solution, the authors define a nominal small length and width for the initial conditions to be applied. Generally, the pressure along the fracture is not known a priori, and it is a part of the solution. Furthermore, with the formation of a fluid-lag or the use of the cohesive model, the pressure singularity is avoided at the tip where the width falls to zero.

The type of flow constitutive response is composed of a tangential and normal flow along the fracture walls.There are two types of coupling that can occur along the fracture depending on whether the fracture walls are assumed permeable or impermeable. For impermeable walls, the fluid pressures in the fracture are converted to equivalent nodal loads and applied appropriately. For permeable walls, the fluid pressure in the fracture must be applied as a pore-pressure and a total stress boundary condition.

For the movement of the fluid in the porous skeleton, with respect to the solid, it is assumed that the diffusion of pore fluid obeys the Darcy law. This classical transport law for isotropic, porous media relates q to the gradient of the fluid pressure p according to Eq. (3) as follows:

$$\mathbf{q} = -k/\mu(\nabla p - \mathbf{f}) \tag{3}$$

where, $\mathbf{q}$ = fluid flux; k = intrinsic permeability (assumed to be constant); μ = fluid viscosity; ∇ = gradient operator and $\mathbf{f}$ are the fluid volume forces. Note that it is assumed that the fluid in the fracture is identical rheologically to the pore fluid.

Rock Deformation

In a fluid saturated formation, the pore fluid-flow and the elastic deformations are coupled. The usual assumption is that the porous materials are saturated with either incompressible or compressible pore fluids. Furthermore, the grains of the solid phase can also be considered either incompressible or compressible. The classical Biot (1941) theory of poro-elasticity attempts to model the mechanical response of a porous material, which has a solid elastic skeleton, with the pore space filled with a viscous fluid. The equations derived by Biot (1941) exhibit an explicit coupling between the dilation of the elastic skeleton and the pressure of the diffusing pore fluid. The governing equations can be derived by using the Darcy flow equation to model the diffusion process, a mass conservation equation for the pore fluid and the equilibrium equation for the stresses. Hence, the fundamental basis of the equations is well founded. However, the assumption of linear elastic behavior of the porous skeleton is a significant limitation in the application of the theory to brittle materials that could exhibit stiffness changes. The poroelastic materials differ from the corresponding quasi-static elastic solids as a time dependence is introduced in the otherwise time-independent elasticity equations. Furthermore, nonlinear behavior can be observed because of the development of microcracks and microvoids in the porous fabric, which essentially retains its elastic nature. Another possible reason for a nonlinear response is the diffusing pore fluid, which can have a large effect under rapid loading as in hydraulic fracturing operations compared to that of a natural diffusion timescale; hence, the material response is stiffer than for slower loadings because the fluid has less time to diffuse away (Atkinson and Craster 1991).

Int. J. Geomech., 2012, 12(2): 160-167

The poroelastic theory is also relevant to the fracture of rocks for enhancing the recovery of hydrocarbons through hydraulic fracturing. It is easily understood that during the initiation and propagation of the fracture, when the fracture is internally pressurized by pumping viscous fluid, the fluid may leak into the formation depending on the formation permeability. This causes a volume expansion of the material around the fracture tending to close the fracture. There are also external stresses and pore-pressure fields, which may affect the hydraulic fracture. Therefore, a complicated interaction exists between the diffusing pore fluid and applied loading, which must be computed numerically because such analytical solutions are impossible to obtain.

The basic theory of poro-elasticity in which the resulting fully coupled linear quasi-static field equations were derived, was initially introduced by the pioneering work of Biot (1941); since then, many researchers have contributed to its further development. A comprehensive review of the theory of poro-elasticity can be found in Detournay and Cheng (1993). The theory is commonly applied to soil mechanics problems especially for consolidation problems. The elastic response of the porous medium is given by the elastic strain rate and the elastic fluid mass content. These two parameters are related to the rates of total stress $\dot{\sigma}$ and pore-pressure $\dot{p}$ through isotropic constitutive equations that involve four material coefficients, namely: (1) the drained young's modulus ($E > 0$), (2) the drained Poisson ratio ($v \in [-1, 0.5]$), (3) the undrained Poisson ratio ($v_u \in [v, 0.5]$), and (4) the Skempton coefficient ($B > 0$). The aforementioned restrictions on the material parameters according to Rice and Cleary (1976) ensure positive definiteness of the elastic constitutive equations in terms of the strain and stress pairs (ε, ζ), (σ, p). By definition, the total stresses are related to the effective stresses through the following:

$$\sigma'_{ij} = \sigma_{ij} - ap\delta_{ij} \tag{4}$$

where, σ'_{ij} = effective stress; and δ_{ij} = kronecker delta, which is assumed to govern the deformation and failure of the rock. The poroelastic Biot-Willis constant α, is independent of the fluid properties, and it is defined as

$$a = \frac{3(v_u - v)}{B(1-2v)(1+v_u)} = 1 - \frac{K}{K_s} \tag{5}$$

As it has been mentioned before, this theory is commonly applied in soils. An important distinction when applying the formulation to rock is that the compressibility of the constitutive materials must be considered. For soils, B and α are equal to unity but in rocks are significantly less than one.

For the linear elastic case, the constitutive relation may be expressed as a linear relation between small changes in strain and small changes in the effective stressesas follows:

$$d\varepsilon = \mathbf{D}_e : d\boldsymbol{\sigma}' \tag{6}$$

Fracture Propagation Criterion

The criteria for fracture propagation are usually given by the conventional energy release rate approach, which states that a fracture propagates when the stress intensity factor at the tip exceeds the rock toughness. For nonlinear mechanics, the most robust criterion is described by the constitutive model of the cohesive zone (Barenblatt 1962; Hillerborg et al. 1976). The cohesive zone model approach should be clearly contrasted with the conventional fracture mechanics on the basis of infinitely sharp fracture models; as such, fracture models have led to a physically meaningless singular stress field near the fracture tip. The cohesive zone is a region ahead of the crack tip that is characterized by microcracking along the crack path. The main fracture is formed by inter-connection of these microcracks (Labuz et al. 1985). The cohesive zone model implies that normal stress continues to be transferred across a discontinuity, which may or may not be visible as shown in Fig. 1. This stress is determined from the softening traction-displacement relation that various rocks exhibit in calibration tests. This traction, which is a function of the separation, falls to zero at a critical opening, and then the fracture propagates. The evolution of the crack is governed by the energy balance between the work of the external loads, the sum of the bulk energy of the uncracked part, and the energy dissipated in the fracture process. A main mathematical difficulty is given by the fact that the fracture energy depends on the opening of the crack. To overcome the mathematical difficulties, it is assumed that the cohesive zone localizes, because of its softening behavior, into a narrow band ahead of the visible crack.

Simple cohesive zone models can be described by two independent parameters that are usually the strain energy G_{IC} and either the tensile strength σ_t or the separation length δ_{IC}. An additional parameter in these models is the slope of the initial loading, which may define a range from rigid-softening to an elastic-softening response under tensile stress-states. The area under the stress-displacement curve equals the strain energy release rate G_{IC} of the material. For elastic solids, this energy is related to the rock fracture toughness K_{IC} through (Kanninen and Popelar 1985) the following:

$$K_{IC}^2 = \frac{G_{IC}E}{1-\nu^2} \tag{7}$$

where, E = young modulus; and ν = Poisson ratio. The rock fracture toughness can be calculated from laboratory tests.

For the case of the rigid-softening behavior, the stress-displacement relation is uniquely determined by the following:

$$\sigma = \sigma_t(1 - \delta/\delta_{IC}) \tag{8}$$

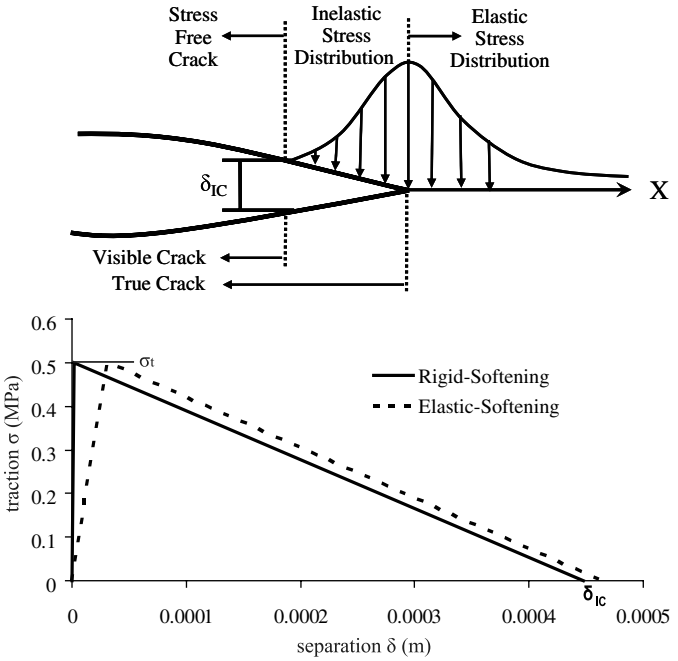

Fig. 1. Representation of the fracture process and the constitutive cohesive zone laws

Int. J. Geomech., 2012, 12(2): 160-167

where, σ_t = uniaxial tensile strength of the rock; and δ_{IC} = critical opening displacement at which σ falls to zero. The value of δ_{IC} is given by the following (Papanastasiou 1999b):

$$\delta_{IC} = \frac{2K_{IC}^2(1-\nu^2)}{E\sigma_t} \tag{9}$$

The previous relations can be augmented and modified to take into account the initial part of the loading curve, which corresponds to linear elastic deformation as follows:

$$\sigma = \sigma_t(\delta/\delta_{el}) \tag{10}$$

where, the limit of elastic deformation is given by the following

$$\delta_{el} = \sigma_t/k_n \tag{11}$$

k_n is the stiffness of the stress-displacement relation in the loading regime with units of [MPa/m]. In the postpeak softening regime the deformation is given by the following:

$$\sigma = \sigma_t\left[1 - \frac{(\delta - \delta_{el})}{(\delta_{IC} - \delta_{el})}\right] \tag{12}$$

Researchers usually choose to ignore such ductile behavior because of the usual instability that numerical codes present when they have to deal with sudden fracture length extensions, which is a direct result of the nonproportional loading, which is the real load-case in hydraulic fracture operations.

Different types of models have been used to represent the mechanical behavior of the cohesive zones. Sarris and Papanastasiou (2011) have investigated the main characteristics of this curve by carrying out computations for different initial slopes to simulate a brittle-to-ductile behavior or more strictly defined from rigid-softening to elastic-softening behavior. They found that for a brittle behavior model, the generated fluid pressures and the resulting fracture aperture were lower than in the case of ductile behavior. The physical interpretation of this analysis applies to soft rocks where larger pressures are needed to propagate the fracture because the generated cohesive zones are larger and the resulting fracture apertures are also larger.

Numerical Implementation

The theory of poro-elasticity can be approximated numerically by using the finite element method and a standard Galerkin formulation as described by Zienkiewicz (1984) and Lewis and Schreffler (2000). Governing equations are discretized in space by the finite element method and in time by the finite difference method. The generalized discrete finite element equations that also account for transient behavior are described hereafter at the element level. Adopting the Lewis and Schreffler (2000) notation, the final equations yield the following:

$$\begin{bmatrix} \theta\mathbf{K}_e & \theta\mathbf{Q} \\ \mathbf{Q}^{\mathrm{T}} & \mathbf{S} + \mathrm{d}t\theta\,\mathbf{H} \end{bmatrix}_{n+\theta} \begin{Bmatrix} \overline{\mathbf{u}} \\ \overline{\mathbf{p}}^f \end{Bmatrix}_{n+1} = \begin{bmatrix} (\theta-1)\mathbf{K}_e & (1-\theta)\mathbf{Q} \\ \mathbf{Q}^{\mathrm{T}} & \mathbf{S} - (1-\theta)\mathrm{d}t\mathbf{H} \end{bmatrix}_{n+\theta} \begin{Bmatrix} \overline{\mathbf{u}} \\ \overline{\mathbf{p}}^f \end{Bmatrix}_{n} + \begin{Bmatrix} \mathbf{f}^u \\ \mathrm{d}t\mathbf{f}^p \end{Bmatrix}_{n+\theta} \tag{13}$$

where, $\mathbf{K}_e$ = elastic stiffness matrix; $\mathbf{Q}$ = coupling matrix; $\mathbf{H}$ = permeability matrix, $\mathbf{S}$ = compressibility matrix; $\mathbf{f}^u$ = forces resulting from displacements; and $\mathbf{f}^p$ = forces resulting from pressures. θ, is the time operator that defines the type of numerical method used to approximate the time in the equations, $0 \le \theta \le 1$. Eq. (13) can be decomposed into the following matrices to account for both, stiffness and flow equations:

$$\begin{aligned}
\mathbf{B} &= \mathbf{L}\mathbf{N}_u \text{ (Strain Operator)} \\
\mathbf{K}_e &= \int_\Omega \mathbf{B}^{\mathrm{T}}\mathbf{D}_e\mathbf{B}\mathrm{d}\Omega \text{ (Linear Elastic Stiffness Matrix)} \\
\mathbf{Q} &= \int_\Omega \mathbf{B}^{\mathrm{T}}\alpha m\mathbf{N}_p\mathrm{d}\Omega \text{ (Coupling matrix)} \\
\mathbf{H} &= \int_\Omega (\nabla\mathbf{N}_p)^{\mathrm{T}}\frac{k}{\mu}\nabla\mathbf{N}_p\mathrm{d}\Omega \text{ (Permeability matrix)} \\
\mathbf{S} &= \int_\Omega \mathbf{N}_p^{\mathrm{T}}\left(\frac{1}{Q'}\right)\mathbf{N}_p\mathrm{d}\Omega \text{ (Compressibility matrix)} \\
\frac{1}{Q'} &= \frac{a-n}{K_s} + \frac{n}{K_f} \\
f^u &= \int_\Omega \mathbf{N}_u^{\mathrm{T}}[\rho^s(n-1) + \rho^f n]g\mathrm{d}\Omega + \int_{\Gamma_u^q} \mathbf{N}_u^{\mathrm{T}}\bar{t}\mathrm{d}\Gamma \\
f^p &= \int_\Omega (\nabla N_p)^{\mathrm{T}}\frac{\mathbf{k}}{\mu}\rho^f g\mathrm{d}\Omega - \int_{\Gamma_w^q} N_p^{\mathrm{T}}\frac{q^f}{\rho^f}\mathrm{d}\Gamma
\end{aligned} \tag{14}$$

with $\mathbf{N}_u$, $\mathbf{N}_p$ as the shape functions to account for the displacements and fluid pressures, respectively; $\mathbf{L}$ = differential operator; $\mathbf{D}_e$ = tangential elastic stiffness matrix; n = porosity of the solid phase; ρ^f = density of the fluid; μ = viscosity of the fluid; K_s and K_f = solid and fluid bulk modulus, respectively; and finally, $\mathbf{k}$ = intrinsic permeability.

For the numerical approximation of the aforementioned set of equations, the direct solution of the coupled systems was used because of its rapid convergence even in severely nonlinear cases. The time integration operator in the pore fluid-flow equation is chosen to be the simple one-step method. In fact, to ensure numerical stability for the solution, the backward difference scheme ($\theta = 1$) is chosen to approximate the time-dependent effects in the problem. Eqs. (6), (13), and (14) form the coupled flow-deformation system, which is solved with the Newton iterative method.

The calculations were carried out in Abaqus, a nonlinear finite element code suit of programs (Abaqus 2006). The usual 4-node, plain strain, isoparametric elements were used to model the domain and 6-node cohesive elements to model the fluid-flow in the fracture and the fracturing process. Both types of elements, additionally from their u, v translation d.o.f, are equipped with a pore-pressure d.o.f to account for the fluid saturation in the domain. A one-to-one correspondence exists between the plain strain flow and domain elements at the corner nodes along the fracture path, ensuring that the fluid mass is conserved across their interface. The two additional nodes in the cohesive elements, positioned in their center, are used to simulate the fluid-flow during the propagation. The fluid-flow can be modeled considering only tangential flow to the crack faces (1D) or tangential and normal flow to the crack faces (2D). The numerical model for the fluid-flow is constructed for the complete length of the predetermined fracture path. The geometry and the resulting discretization are shown in Fig. 2. No special remeshing scheme was used because the mesh was defined to be sufficiently fine along the fracture. The descritized domain was considered to be 30×30 m and the predefined path of the fracture was defined to be 11 m only (cohesive elements) to save computational time. The wellbore location, which is represented by the injection point, is located at the left-lower corner (0, 0) of Fig. 2.

The in situ total stresses were generated as initial stresses and by applying the same values as external equilibrium loads at the far end edges. At the top edge, a value of $\sigma_3 = 3.7$ MPa was considered as the minimum in situ stress, and at the right side of the models a value of $\sigma_1 = 14$ MPa was considered as the maximum in situ

Int. J. Geomech., 2012, 12(2): 160-167

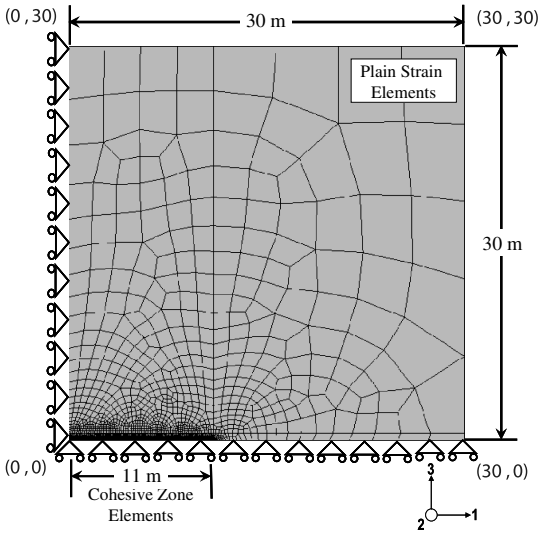

Fig. 2. Geometry, boundary conditions, and discretization of the domain

stress. An initial value of 1.85 MPa was applied for the pore-pressure degree of freedom. These initial conditions were applied to obtain a well-posed system and to achieve system equilibrium before the propagation starts from an initial fracture length of 0.1 m approximately equal with the assumed perforation length.

Analysis and Results

The numerical values of the input data upon which the numerical computations were based are summarized in Table 1. The properties of the cohesive zone are also summarized at the end of the Table. The fracture energy, which is the area under the traction-displacement curve, corresponds to an equivalent fracture toughness of 2 MPa.m$^{0.5}$.

Fig. 3 shows the half-width of a propagating fracture in elastic (dashed line) and poroelastic (solid line) solids. The k_n (×5) mark in the figure means that the initial loading slope of the cohesive model was 5 times the one given in Table 1. The propagating fracture profiles were plotted for the first 7 m at every 1-m interval. Each fracture profile corresponds to a different pumping time. Longer fractures and wider profiles correspond to greater pumping times because the same injection rate was used for a comparison of the results. It is evident that the poroelastic fracture is much wider than the elastic fracture. The cusping of the fractures appears to be larger in the poroelastic case, which means that the cohesive zone that is generated is larger.

Fig. 4 shows the fluid pressures for propagating the previous poroelastic fracture. The fluid pressures that drive the fracture are highly positive along the visible fracture. In the area far-ahead of the propagating tip, the fluid pressure approaches the value of the imposed initial pore-pressure condition.

Fig. 5 shows the net-pressures that are needed to propagate the fractures for the elastic and porous-elastic media as the fracture grows. The net-pressure is descending as the fracture propagates away from the wellbore and reaches almost a steady value a few meters away from the wellbore. Higher pressures are needed to propagate the porous-elastic than the elastic fractures. This difference is more pronounced in the area near the wellbore for short fractures. For short fractures, the cohesive process zone is significant

Table 1. Input Parameters for the Computational Examples

Variable	Value
Rock properties	
Young modulus, E (MPa)	16200
Poisson ratio, ν	0.3
Compressibility, K_s (Pa)	2.5E-10/5E-10
Pumping parameters	
Viscosity, μ (kPa.sec)	0.0001
Injection rate, q (m^3/sec .m)	50E-06/500E-06/5,000E-06
Domain permeability, k (m/sec)	5.88E-08/5.88E-10/5.88E-12
In situ stress field (effective)	
Maximum, σ_1 (MPa)	14
Intermediate, σ_2 (MPa)	9
Minimum, σ_3 (MPa)	3.7
Initial conditions	
Void ratio, e	0.333
Pore-pressure (MPa)	1.85
Initial gap (perforation)-(m)	0.1
Cohesive zone properties	
Tensile strength, σ_t (MPa)	0.5
Loading stiffness k_n (MPa/m)	16200
Fracture cohesive energy, $J_{IC} = G_{IC}$ (kPa.m)	0.224
Permeability of cohesive zone q_b (m/sec)	5.88E-08/5.88E-10/5.88E-12

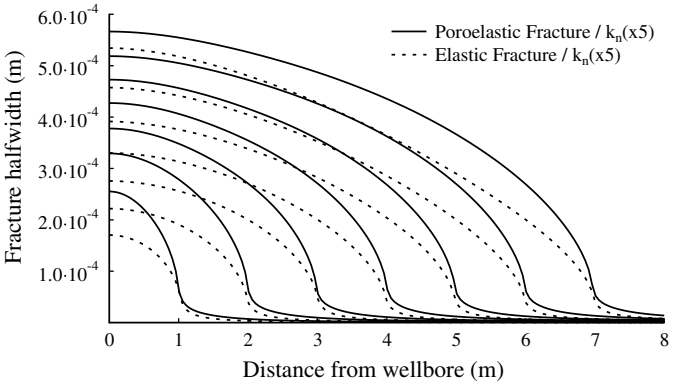

Fig. 3. Comparison of propagating fractures

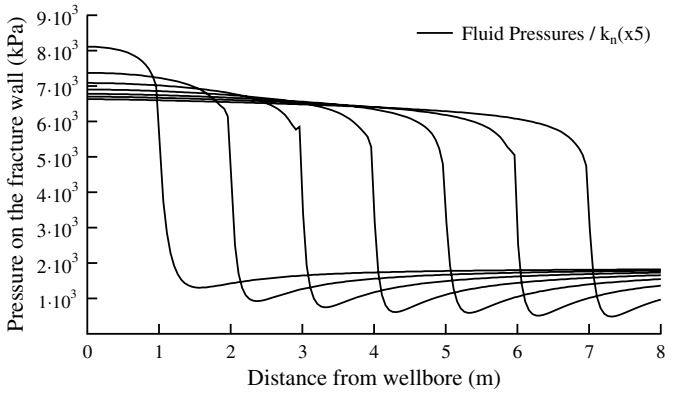

Fig. 4. Fluid pressures for the poroelastic case

Int. J. Geomech., 2012, 12(2): 160-167

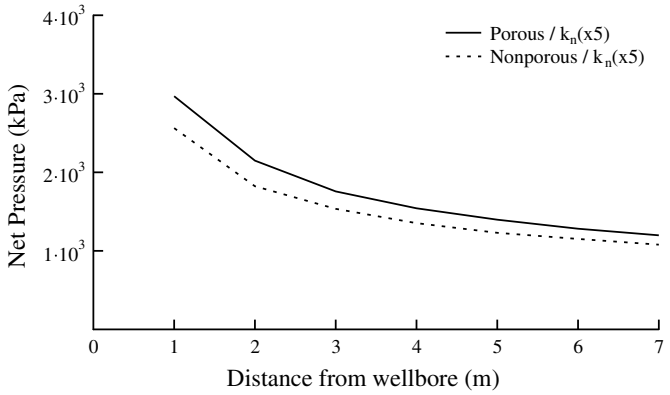

Fig. 5. Comparison of porous and nonporous net-pressures

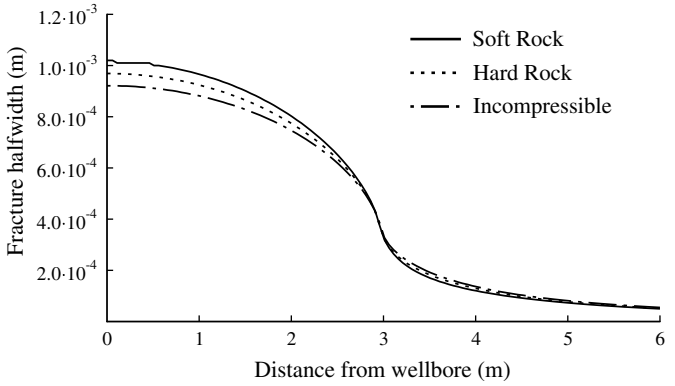

Fig. 7. Comparison of porous compressible fractures for the elastic-softening case

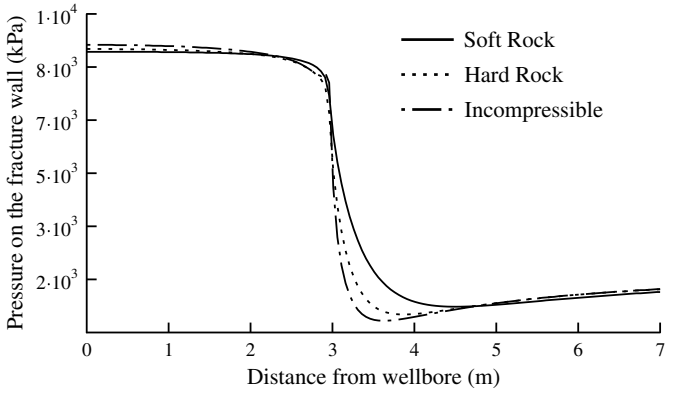

Fig. 8. Comparison of fluid pressures in porous compressible fractures for the elastic-softening case

compared to the fracture length; whereas, as the fracture grows, the process zone becomes insignificant to the fracture length.

Fig. 6 shows that the size of the cohesive zone that is created is larger in the poroelastic fracture, which is also consistent with the difference in the fracture apertures (Fig. 3). The large process zone that is observed in the poroelastic case is also consistent with the elevated net-pressures that are observed in Fig. 5. Therefore, it is concluded that the net-pressures needed to propagate fractures in cohesive mediums are proportional to the size of the created cohesive zone. When the size of the cohesive zone is relatively small, the net-pressure that is needed to propagate the fracture is comparable to the elastic case, even in the case of the poroelastic fracture.

For a further analysis of the porous continuum, a parametric analysis was conducted for the role of the rock compressibility. The grain compressibility is defined as the ratio of a fractional volume change with respect to a pressure change. In the simulations described subsequently, only the compressibility of the solid grains were considered, and the numerical values were selected from the literature (Detournay and Cheng 1993) to correspond to soft rock, hard rock, and incompressible rock. Fig. 7 presents the comparison of poroelastic fracture profiles that correspond to soft, hard, and incompressible rock formations. Fig. 7 shows that the fracture aperture is wider in the case of the soft formation followed by the hard and incompressible formations. This expected small difference is attributed to the fact that the grain compressibility values that were chosen have a narrow span for a physical meaning and not extreme unrealistic values for the purpose of the simulation (Table 1).

Fig. 8 shows the fluid pressures needed to propagate the fracture at the respective distance of 3 m from wellbore. A small difference exists in the fluid pressures that are responsible for propagating the fractures. As mentioned before, this can be attributed to the small range of numerical values of compressibilities that were chosen to have a physical meaning. However, if a closer look at Fig. 8 is taken, ahead of the visual fracture tip, it is shown that a redistribution of pore-pressure fields exists that affects the size of the cohesive zone caused by the extra volumetric strain—(p/K_s) that was enforced by changing the bulk modulus of the solid grains.

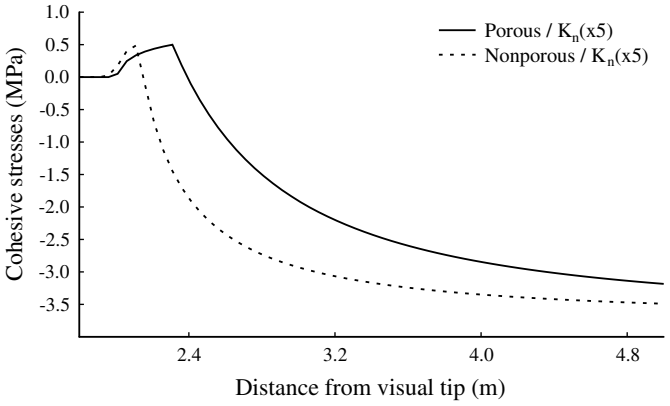

Fig. 6. Comparison of porous and nonporous cohesive stresses

Previous research works have outlined the importance of hydraulic fracturing in porous and fluid saturated domains and the role of formation permeability and the propagation velocity focusing on the fluid-lag and the near-tip area of a propagating fracture (Detournay and Garagash 2003). In this work, the influence of permeability on the pressure gradients globally, including the cohesive zone, is investigated. Values were chosen to correspond to a high permeability and a low permeability rock, and a small injection rate was considered to make the problem independent of the propagation velocity. According to the Darcy law, the ratio κ/μ appears in the diffusion Eq. (3), which means that an increase in the permeability will have the same effect as an equivalent decrease in the fluid viscosity. Fig. 9 presents the fracture apertures of a propagating fracture in a poroelastic medium after the visible fracture had reached a length of 5 m. It is shown that the aperture in the body of the fracture is wider in the case where the formation is highly permeable.

Fig. 10 presents the fluid pressures needed to propagate the fracture for the respective fracture apertures of Fig. 9.

It appears that the fluid pressures are larger in the case of the highly permeable rock formation. In the near-tip area in front of the

Int. J. Geomech., 2012, 12(2): 160-167

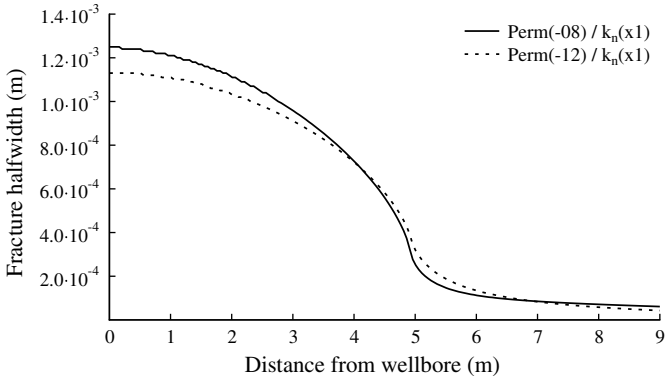

Fig. 9. Comparison of porous fractures with different permeabilities

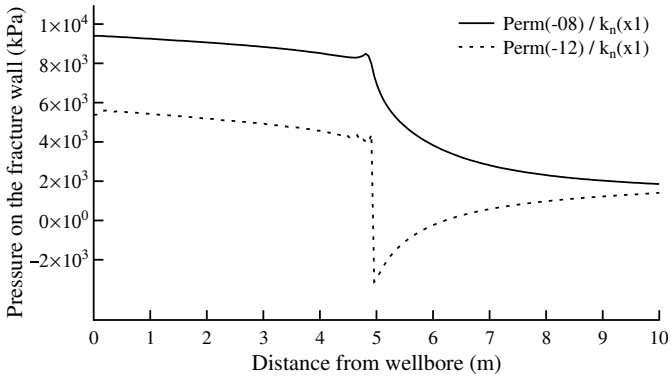

Fig. 10. Comparison of porous fluid pressures with different permeabilities

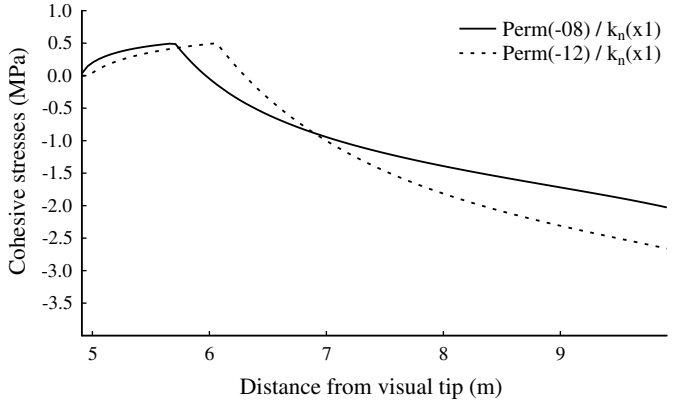

Fig. 11. Comparison of cohesive stresses with different permeabilities

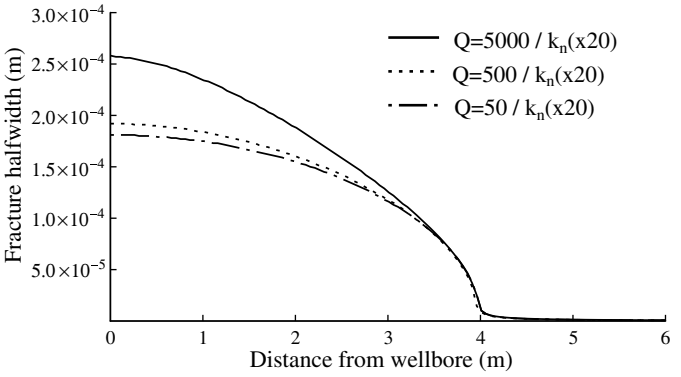

Fig. 12. Comparison of porous fractures for different injection rates

propagating fracture, the pore-pressure presents a smooth descending toward the far-field initial condition. This reveals that because of a slow injection rate and high permeability, the fracture fluid had enough time to diffuse in the cohesive zone increasing the pressure gradient and creating, in its turn, the wider fracture apertures. A further examination of the fluid for the case of the low permeability rock in the area near the tip shows a strong redistribution of the pore-pressure field resulting in a highly negative sign in the cohesive zone. Despite the low injection rate and slow propagation, the fluid had not enough time to invade the rock formation that was practically impermeable creating negative pore-pressure at the fluid front position. This, of course, through the definition of the effective stress, is responsible for the creation of a larger cohesive zone (Fig. 11). Furthermore, such highly negative signs in the fluid pressures may also imply that suction takes place in the near-tip area of the propagating fracture.

Next, the influence of the propagation velocity was investigated. For an impermeable formation, it is expected that the propagation velocity is directly linked to the injection rate. The numerical value of the permeability was changed to correspond to a partly permeable rock formation. Three different values of injection rates were considered. Fig. 12 presents the fracture aperture of a propagating fracture with different injection rates to correspond to slow, intermediate, and fast propagation velocity in a poroelastic medium. The fracture was left to propagate up to 4 m to allow the fracture and the fluid pressures to evolve in time (no early time solution) and space. The resulting fracture aperture is wider for the fast propagation.

Fig. 13 presents the fluid pressures needed to propagate the fractures with the different velocities for the respective fracture apertures shown in Fig. 12. The fluid front is found to be where the fluid pressures change sign. It is observed that in front of the propagating fracture in a near-tip area, a highly negative value of fluid pressure exists for all propagation velocities. This has the physical meaning of pore fluid suction that takes place during the fracture propagation. It appears that the fluid pressures are slightly larger in the area near the wellbore in the case of fast propagation followed by the intermediate and slow fracture propagation velocity. Despite the small differences in the propagation pressures, the obtained width profile for the slow propagation case is narrower primarily because of the developed back stresses in the body of the fracture.

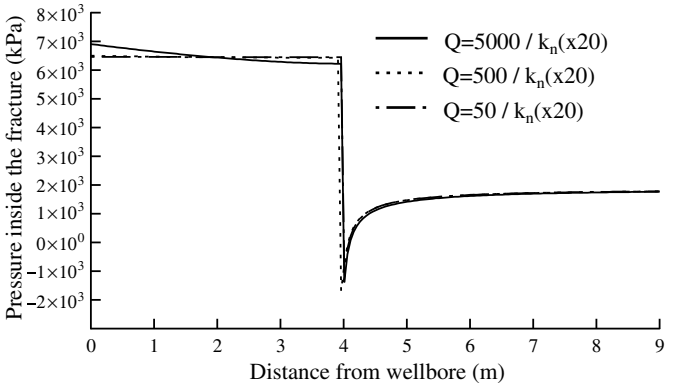

Fig. 13. Comparison of porous fluid pressures for different injection rates

Int. J. Geomech., 2012, 12(2): 160-167

Conclusions

Numerically hydraulic fracturing was studied in a poroelastic cohesive rock formation. The objective was to investigate the elevated pressures that are needed to propagate the fractures in the field as compared to conventional model predictions. It was found that the fluid pressures and the fracture apertures are larger in the case of a high permeability formation. The influence of the grain compressibility has a limited effect on fluid pressures and fracture dimensions. Wider fracture profiles are obtained with high injection rates that correspond to fast propagation and narrower fractures, in the case of low injection rate or slow propagation, although the differences in the propagation pressure is relatively small. This result is attributed to the developed back-stress in the body of the fracture in the latter case. These findings suggest that the additional mechanism of fluid-flow diffusion from the fracture and the size of the cohesive zones must be taken into account in hydraulic fracture modeling because they may explain differences in the net-pressures between field measurements and model predictions.

Acknowledgments

The authors would like to thank the Cyprus Research Promotion Foundation for funding this research through the program ENISX/0505/31.

References

Abaqus. (2006). *Version 6.6 Theory Manual*, Abaqus, Providence, RI.

Adachi, J., and Detournay, E. (2008). "Plain strain propagation of a hydraulic fracture in permeable rock." *Eng. Fract. Mech.*, 75(16), 4666–4694.

Atkinson, C., and Craster, R. V. (1991). "Plane strain fracture in poroelastic media." *Proc. R. Soc. London, Ser. A*, 434(1892), 605–633.

Barenblatt, G. I. (1962). "The mathematical theory of equilibrium cracks in brittle fracture." *Adv. Appl. Mech.*, 7, 55–129.

Biot, M. A. (1941). "General theory of three dimensional consolidation." *J. Appl. Phys.*, 12(2), 155–164.

Carbonell, R., Desroches, J., and Detournay, E. (1999). "A comparison between a semi-analytical and a numerical solution of a two-dimensional hydraulic fracture." *Int. J. Solid. Struct.*, 36(31–32), 4869–4888.

Desroches, J., Detournay, E., Lenoach, B., Papanastasiou, P., Pearson, J. R.A., Thiercelin, M., and Cheng, A. (1994). "The crack tip region in hydraulic fracturing." *Proc. R. Soc. London, Ser. A*, 447(1929), 39–48.

Detournay, E. (2004). "Propagation regimes of fluid-driven fractures in impermeable rocks." *Int. J. Geomech.*, 4(1), 35–45.

Detournay, E., and Cheng, A. H-D. (1993). "Fundamentals of poroelasticity." *Comprehensive rock engineering: Principles, practice and projects*, J. A. Hudson, ed., Vol. 2, Pergamon, Oxford, UK, 113–171.

Detournay, E., and Garagash, D. I. (2003). "The near-tip region of a fluid-driven fracture propagating in a permeable elastic solid." *J. Fluid Mech.*, 494, 1–32.

Garagash, D., and Detournay, E. (2000). "The tip region of a fluid-driven fracture in an elastic medium." *J. Appl. Mech.*, 67(1), 183–192.

Germanovich, L. N., Astakhov, D. K., Shlyapobersky, J., Mayerhofer, M. J., Dupont, C., and Ring, L. M. (1998). "Modeling multi-segmented hydraulic fracture in two extreme cases: No leak-off and dominating leak-off." *Int. J. Rock Mech. Min. Sci.*, 35(4–5), 551–554.

Hillerborg, A., Modeer, M., and Petersson, P. E. (1976). "Analysis of crack formation and crack growth in concrete by means of fracture mechanics and finite elements." *Cem. Concr. Res.*, 6(6), 773–782.

Jeffrey, R. G., Settari, A., Mills, K. W., Zhang, X., and Detournay, E. (2001). "Hydraulic fracturing to induce caving: Fracture model development and comparison to field data." *Proc., 38th US Rock Mechanics Symp.*, Vol. 1, Balkema, Lisse, The Netherlands, 251–259.

Kanninen, M. F., and Popelar, C. H. (1985). "Advanced fracture mechanics." Oxford Univ., UK.

Labuz, J. F., Shah, S. P., and Dowding, C. H. (1985). "Experimental analysis of crack propagation in granite." *Int. J. Rock Mech. Min. Sci. Geomech. Abstr.*, 22(2), 85–98.

Lecampion, B., and Detournay, E. (2007). "An implicit algorithm for the propagation of hydraulic fracture with a fluid lag." *Comp. Meth. Appl. Mech. Eng.*, 196(49–52), 4863–4880.

Legarth, B., Huenges, E., and Zimmermann, G. (2005). "Hydraulic fracturing in sedimentary geothermal reservoir: Results and implications." *Int. J. Rock Mech. Min. Sci.*, 42(7–8), 1028–1041.

Lewis, R. W., and Schreffler, B. A. (2000). "The finite element method in the static and dynamic deformation and consolidation of porous media." Wiley, New York.

Logan, J. M., Rudnicki, J. W., Wawersik, W. R., and Wong, T. (2000). "Geomechanics perspective in terrestrial sequestration of CO2: An assessment of research needs." *Adv. Geophys.*, 43, 97–177.

Murdoch, L. C., and Slack, W. W. (2002). "Forms of hydraulic fractures in shallow fine grained formations." *J. Geotech. Geoenviron. Eng.*, 128(6), 479–487.

Papanastasiou, P. (1997). "The influence of plasticity in hydraulic fracturing." *Int. J. Fract.*, 84(1), 61–79.

Papanastasiou, P. (1999a). "The effective fracture toughness in hydraulic fracturing." *Int. J. Fract.*, 96(2), 127–147.

Papanastasiou, P. (1999b). "An efficient algorithm for propagating fluid driven fractures." *Comp. Mech.*, 24(4), 258–267.

Papanastasiou, P., and Thiercelin, M. (1993). "Influence of inelastic rock behavior in hydraulic fracturing." *Int. J. Rock Mech. Min. Sci. Geomech. Abstr.*, 30(7), 1241–1247.

Rice, J. R., and Cleary, M. P. (1976). "Some basic stress diffusion solutions for fluid-saturated elastic porous media with compressible constituents." *Rev. Geophys. Space Phys.*, 14(2), 227–241.

Sarris, E., and Papanastasiou, P. (2011). "The influence of cohesive process zone in hydraulic fracturing modelling." *Int. J. Fract.*, 167(1), 33–45.

Savitski, A., and Detournay, E. (2002). "Propagation of a fluid-driven penny-shaped fracture in an impermeable rock: Asymptotic solutions." *Int. J. Solid Struct.*, 39(26), 6311–6337.

van Dam, D. B., Papanastasiou, P., and de Pater, C. J. (2002). "Impact of rock plasticity on hydraulic fracture propagation and closure." *SPE Prod. Facil.*, 17(3), 149–159.

Zhang, X., Jeffrey, R., and Detournay, E. (2005). "Propagation of hydraulic fracture parallel to a free-surface." *Int. J. Numer. Anal. Methods Geomech.*, 29(13), 1317–1340.

Zienkiewicz, O. C. (1984). "Coupled problems and their numerical solution." *Numerical methods in coupled systems*, Wiley, New York.